Astron. Astrophys. 341, 201–210 (1999)

ASTRONOMY AND ASTROPHYSICS

Microlensing of circumstellar envelopes

I. Simplified considerations for diagnosing radial and azimuthal flow

R. Ignace and M.A. Hendry

Kelvin Building, Department of Physics and Astronomy, University of Glasgow, Glasgow G12 8QQ, Scotland, UK

Received 16 July 1998 / Accepted 15 September 1998

Abstract. This paper presents first results on the line profile shapes from a circumstellar envelope in bulk motion as modified by a microlensing event. Only geometrically and optically thin spherical shells in uniform expansion or rotation are considered here so as to emphasise the information content available in the profile shapes. In particular it is demonstrated that for the case of expansion, the line emission can increase by significant factors and the time variation of the profile shape is *symmetric* about line centre. For uniform rotation the line emission also increases significantly, but the time evolution of the profile shape is distinctly *asymmetric*. Thus, microlensing is seen to yield information about the velocity field in the extended envelope. We elaborate on (a) the observational advantages of tailoring microlensing programs toward detecting extended circumstellar envelopes, (b) the use of multiline observations to infer other properties of the envelopes, such as the ionization stratification, (c) the use of the continuum excess emission at infrared wavelengths as a means of probing the envelope structure, and (d) the use of polarisation for constraining the properties of "clumpy" winds.

Key words: cosmology: gravitational lensing – galaxies: quasars: emission lines – stars: rotation – stars: imaging – stars: circumstellar matter – line: profiles

1. Introduction

In recent years the phenomenon of gravitational microlensing has emerged as a powerful new tool for analysing the distribution and nature of the dark matter in the halo of the Milky Way. Since the pioneering suggestion by Paczyński (1986) that the systematic monitoring of several million stars in the LMC and Galactic bulge could be an effective method for detecting halo dark matter, a number of different monitoring programs have been established and several hundred candidate microlensing events detected (Alcock et al. 1993, 1996; Aubourg et al. 1993; Udalski et al. 1993, 1994).

In addition to the detection of dark matter, microlensing studies have led to significant advances in other areas of astrophysics. The huge quantity of data from the monitoring programs has revealed many thousands of new variable stars, prompting important developments in understanding the physics of Cepheids (Alcock et al. 1995), RR Lyraes (Alcock et al. 1998), and eclipsing binaries (Grison et al. 1995). In the past few years several authors have pointed out that the microlensing events themselves can in principle yield much useful information about the stars *being lensed*, in the case where the stars have significant angular extent (c.f., Gould 1994; Valls-Gabaud 1994, 1998; Simmons et al. 1995a; Sasselov 1997; Hendry et al. 1998; Hendry & Valls-Gabaud in prep). Although the majority of candidate events display light curves which are well-fitted by a simple point source model, the MACHO collaboration has reported clear evidence of a microlensing event that exhibits extended source effects (Alcock et al. 1997). Thus, theoretical consideration of the microlensing of extended sources has become a timely issue.

The characteristic scale for microlensing is usually taken to be the Einstein radius of the lens, defined as

$$R_{\rm E} = \left[\frac{4GM}{c^2}\frac{(D_{\rm S}-D_{\rm L})D_{\rm L}}{D_{\rm S}}\right]^{1/2} \tag{1}$$

where M is the lens mass, and $D_{\rm S}$ and $D_{\rm L}$ are the distance to the source and lens, respectively. In the microlensing literature it is customary to replace spatial separations with *angular* separations, conveniently expressed in units of the angular Einstein radius, $r_{\rm E}$, namely

$$r_{\rm E} = R_{\rm E}/D_{\rm L} = \left[\frac{4GM}{c^2}\frac{(D_{\rm S}-D_{\rm L})}{D_{\rm L}D_{\rm S}}\right]^{1/2} \tag{2}$$

In the case of a point source lensed by a point mass, the amplification, A, of the source (i.e., the ratio of lensed to unlensed flux)[1] can be shown to depend only on the *projected* angular separation d of the lens and source, expressed in units of $r_{\rm E}$ of the lens (c.f., Paczyński 1986; 1996), namely

$$A(d) = \frac{d^2+2}{d\sqrt{d^2+4}} \tag{3}$$

Send offprint requests to: rico@astro.gla.ac.uk

[1] Strictly speaking, since lengths are usually expressed in terms of angular distance, the expressions derived for the lensed and unlensed fluxes are often in non-standard units, but one is typically concerned with the ratio of lensed to unlensed fluxes, so that the units cancel for the degree of amplification.

Eq. (3) is independent of the observed wavelength of the source – indeed the achromaticity of the light curve shape is one of the principal defining characteristics of a microlensing event, usually allowing contamination by variable stars to be identified in monitoring programs. However, in the case of an extended source where the angular stellar radius R_* is non-negligible as compared to the $r_{\rm E}$ of the lens, the light curve shape does depend on both the value of R_* and the waveband of observation (Gould 1994; Simmons et al. 1995a; Sasselov 1997; Valls-Gabaud 1998). This chromatic signature arises principally because of the wavelength dependence of limb darkening: the lens "sees" a star with an effective angular radius that changes with wavelength. Far from being a problem, these extended source effects have been promoted as a virtue in microlensing studies, since they offer a means to better constrain the distance, mass and transverse velocity of the lens (c.f., Simmons et al. 1995a; Alcock et al. 1997). More interesting in the present context, however, has been the proposal that the microlensing of extended sources can be used as a probe of stellar atmospheres, since the shape of the light curve at different wavelengths carries information on the radial surface brightness profile of the source (c.f., Gould 1994; Simmons et al. 1995a; Peng 1997; Valls-Gabaud 1998).

While most authors have considered only the broad-band photometric light curves produced by extended sources, some recent work has focussed on the additional information provided by polarimetric and spectroscopic observations. Simmons et al. (1995a) and Simmons et al. (1995b) considered the limb polarisation of spherically symmetric electron scattering stellar atmospheres as lensed by a point mass, and showed that maximal polarisations of order one percent can be achieved during the event – well within the capabilities of present-day detection for giant stars at the distance of the LMC and Galactic Bulge (Newsam et al. in prep). Coleman (1998) improved this treatment to consider a more general model of a central star surrounded by an extended spherically symmetric scattering envelope, with radially varying density. Newsam et al. (1998) showed that the measurement of polarisation during a microlensing event for such a model could significantly improve the determination of the stellar model parameters, compared with model fits based only on broad-band photometric observations. Valls-Gabaud (1998) has considered the spectroscopic signatures of microlensing from extended sources, and shows that in addition to providing an unambiguous signature of microlensing, spectral diagnostics such as the equivalent width of the Balmer $H\beta$ line can be a powerful means of testing stellar atmosphere models.

However, a major deficiency in the theoretical treatment of extended source effects during a microlensing event is the neglect of extended *circumstellar* envelopes. Although the model developed in Coleman (1998) includes such a scattering envelope, and Simmons et al. (in prep) have further extended this model to the case where the envelope is aspherical (e.g., a Be disk), their computations have been carried out only for the broad-band photometric and polarimetric response to the event, and the time evolution of line profile shapes has not been considered. Heyrovský & Loeb (1997) have considered microlensing of elliptical sources and compute emission profiles from Keplerian disks, but their discussion of line effects focuses on cosmological sources. Although hot stars may be unlikely sources to be lensed, the line emission from hot star winds can be quite strong and typically arise from extended regions of several stellar radii or more, and the amount of emission and the profile shape depend on the velocity field in the flow. In this first paper on the effects of microlensing for circumstellar envelopes, we employ simplified geometries to investigate the potential of microlensing for diagnosing the flow structure from the time evolution of the line profile shapes.

The structure of this paper is as follows. In Sect. 2.1 we derive the unlensed line profile for a shell that is either expanding or rotating. Then in Sect. 2.2, we introduce the effects of microlensing, considering first a direct comparison between the expansion and rotation cases then investigating the effect of varying the angular Einstein radius of the lens and the orientation of the lens trajectory. Finally, in Sect. 3 we discuss implications of our results and future extensions of our work to utilize multiline observations, continuum excess emission and polarimetric measurements as further means of probing the envelope structure.

2. Microlensing of circumstellar envelopes

As a first step in describing the diagnostic benefits of microlensing effects on line profiles formed in circumstellar envelopes, we consider here only the highly simplified case of a geometrically and optically thin spherical shell in uniform expansion or rotation. The star is also approximated as a point source of illumination, hence absorption and occultation effects are ignored. We first describe the line profiles of these two cases in the absence of lensing and following derive results that include microlensing.

2.1. Unlensed profiles from expanding or rotating shells

An important consequence of the optically thin assumption is that the radiative transfer for the line profile reduces to a volume integral over the envelope, because the assumption implies that every photon scattered or produced in the envelope escapes. However, for an envelope in bulk motion such that the flow speed greatly exceeds the thermal broadening, the locus of points contributing to the emission at any particular frequency in the line profile is confined to an "isovelocity zone" (c.f., Mihalas 1978). These zones are determined by the Doppler shift formula, namely

$$\nu_{\rm Z} = \nu_0 \left(1 - \frac{v_{\rm Z}}{c}\right), \tag{4}$$

where the observer's coordinates are (X, Y, Z) with the line-of-sight along Z, $\nu_{\rm Z}$ is the Doppler shifted frequency, and $v_{\rm Z} = -\mathbf{v}(\mathbf{r})\cdot\hat{\mathbf{Z}}$ is the projection of the flow speed onto the line-of-sight (as indicated in Figs. 1 and 2). Note that the stellar coordinates are Cartesian (x, y, z) and spherical (r, ϑ, φ). Eq. (4) will prove crucial for relating the variable profile shape to the kinematics of the envelope.

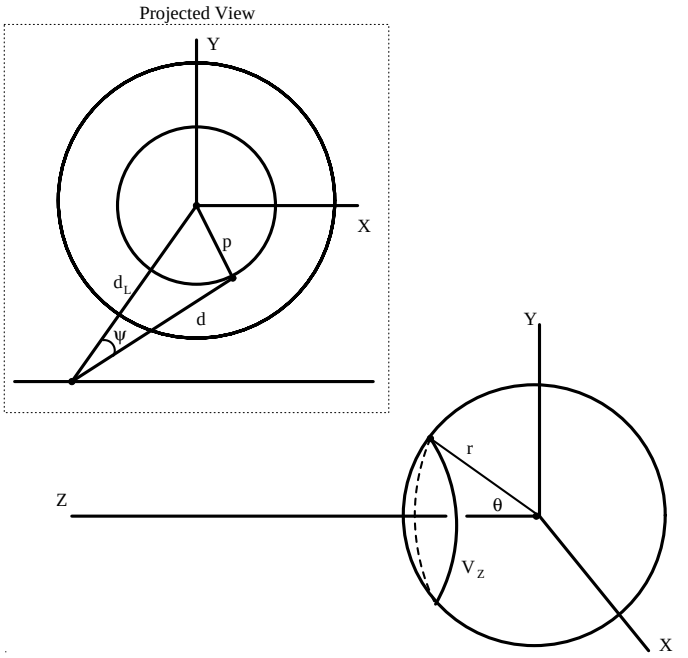

Fig. 1. Shown is the geometry associated with a uniformly expanding shell. Lower right shows the 3-dimensional view with the observer located on the Z–axis. Circular rings centered on that axis are distinguished by their Doppler shift $v_{\rm Z}$. Upper left (boxed) shows the microlensing event in projection, with the lens a distance $d_{\rm L}$ from the shell center.

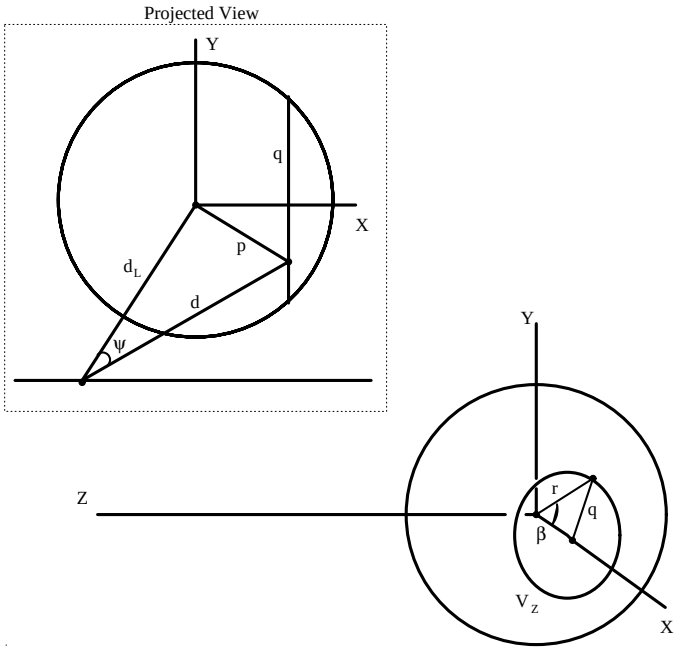

Fig. 2. Shown is the geometry associated with a uniformly rotating shell. The geometry is quite similar to that for an expanding shell, only now the circular ring is centered on the X-axis, with β the opening angle of the ring and q the radius of the ring. In projection the circular ring is seen edge-on thus appearing as a vertical strip.

For constant expansion with $\mathbf{v} = v_0\hat{\mathbf{r}}$, the velocity shift along the observer's line-of-sight becomes $v_{\rm Z} = -v_0\cos\theta$. For $v_{\rm Z}$ constant, the angle θ is also constant, hence the isovelocity zone traces a ring on the surface of the shell, as can be seen in Fig. 1. For intensity I_ν, impact parameter p, and angle α which is measured from X, the observed flux of line emission from the ring is given by

$$F_\nu = \int_0^{2\pi} I_\nu(p)\, p\, dp\, d\alpha = 2\pi\, I_\nu(p)\, p\, dp. \tag{5}$$

Note again that, in accordance with the standard notation adopted in the microlensing literature, all distance scales are in fact taken as angular distances that are normalised to $r_{\rm E}$ of the lens. This implies that the "flux" of Eq. (5) has rather unusual units; however, the results of the microlensed line profile calculations in the following section will be displayed as line ratios of the lensed to unlensed cases, so that the (non-standard) units of flux will cancel.

Eq. (5) is not especially instructive as regards the profile shape. It is therefore worthwhile to derive an analytic result for the line profile. The observed intensity from any point in an isovelocity ring with impact parameter p is $I_\nu(p) = j_\nu(r)dz$, with j_ν the emissivity. The integral expression (5) then becomes

$$F_\nu = \int_{v_{\rm Z}} j_\nu(r)\, dz\, p\, dp\, d\alpha = \int_{v_{\rm Z}} j_\nu(r)\, dV, \tag{6}$$

thus a volume integral over the isovelocity zone, as expected for an optically thin line. In fact using spherical coordinates with $dV = r^2\, dr\, d\mu\, d\alpha$, the flux of line emission reduces to

$$F_\nu = \frac{2\pi\, r^2\, j_\nu(r)}{v_0}\, dr\, dv_{\rm Z}, \tag{7}$$

where we have substituted $d\mu = -dv_{\rm Z}/v_0$ and integrated over $d\alpha$ to obtain the factor of 2π. Since the velocity shift does not appear in this expression, F_ν is derived to be constant with frequency, or flat-topped. The flat-top profile result in this case is well-known, dating back to Menzel (1929). Note that the constancy of F_ν in the line implies that $p\, I_\nu(p)$ from Eq. (5) is likewise constant, a result that will be valuable for numerical calculations of line profiles when microlensing is included.

Now for the case of uniform rotation, the flow velocity is given by $\mathbf{v} = v_0\hat{\varphi}$, for which the velocity shift becomes $v_{\rm Z} = -\sin\vartheta\cos\varphi\sin i$, where i is the viewing inclination defined by $\hat{\mathbf{Z}}\cdot\hat{\mathbf{z}}_* = \cos i$. For the measurement of φ, we take the observer's X–axis to be coincident with the star's x–axis (thus, for a pole-on view, $\alpha = \varphi$). Employing spherical trigonometry, it can be shown that $\cos\beta = \cos\varphi\sin\vartheta$, where β is a spherical polar angle measured from the X–axis. Since the inclination is fixed for a given shell, the isovelocity zones in the rotating case once again reduce to circular rings, but now of opening angle β and concentric about the X–axis.

Since the isovelocity zone is a ring as in the expanding case, it remains that the profile shape is flat-topped in the rotating case. The flux of line emission F_ν for a rotating shell becomes

$$F_\nu = \frac{2\pi\, r^2\, j_\nu(r)}{v_0\sin i}\, dr\, dv_{\rm Z}. \tag{8}$$

The factor $\sin i$ appearing in the denominator is a consequence of the shell velocity being azimuthal instead of spherical. Note

that for increasingly pole-on perspectives, the line flux would appear to diverge; however, an underlying assumption of our derivation is that the thermal broadening of the line can be ignored. For nearly pole-on cases, this assumption is invalid.

It is convenient to define the angular length q as the radius of the ring, similar to p in the expanding case (see Fig. 2). Then just as $pI_\nu(p)$ was a constant for an expanding shell, so $qI_\nu(q)$ is constant for a rotating shell.

We have shown that in the absence of microlensing effects, expanding and rotating shells both produce flat-top profiles and are therefore indistinguishable[2]. However, there are two clear distinctions between the expanding and rotating cases. (a) In the expanding case, the isovelocity ring is circular in projection, but for rotation the ring is viewed edge-on and therefore appears to the observer as a strip of length $2q$. (b) For expansion the shell is front-back symmetric, so that for every ring of velocity shift $v_{\rm Z}$ on the front side of the shell, an exact replica exists on the back side, only with $v_{\rm Z}$ of opposite sign. However, for rotation the symmetry is left-right, so that all the points on the left hemisphere have $v_{\rm Z}$ of the same sign, and all the points on the the right hemisphere also have the same sign but opposite to that on the left. These differences in the ring projection and the distribution of projected Doppler shifts between the two cases will have significant consequences for the evolution of the line profile shape during a microlensing event.

2.2. The effects of microlensing

As discussed in the introduction, the effect of microlensing is to introduce the amplification factor $A(d)$ from Eq. (3) into the flux integral, which now becomes

$$F_\nu = \int A(d)\, I(p)\, p\, dp\, d\alpha, \tag{9}$$

where d is the projected impact parameter from the lens to any differential element of material in the envelope. In Figs. 1 and 2, we further define $d_{\rm L}$ as the impact parameter from the lens to the shell center. The minimum value of $d_{\rm L}$ is denoted by d_0 signifying the minimum impact paramter of the lens trajectory. Note that Eq. (3) is the expression derived for the amplification of a point source lens (c.f., Paczyński 1986), thus the flux reduces to a convolution of the unlensed intensity and the amplification by the points lens, integrated across the source plane. Note that as $d \gg 1$, $A(d)$ tends toward unity, and the unlensed case is recovered.

Using Eq. (9), we have computed emission line profiles for shells in either uniform expansion or rotation. Table 1 summarises the simulations that are shown in Figs. 3–7. In Table 1, the parameter γ defines the orientation of the lens trajectory (c.f., Sect. 2.2.3), $A_{\rm max}$ is the maximum amplification at any frequency in the profile during the microlensing event, and $f_{\rm line}$ is the maximum enhancement of the *total* line emission during the microlensing event relative to that in the absence of lensing. The following sections describe the consequence of the microlensing as it relates to (a) the flow velocity field, (b) the Einstein radius of the lens, and (c) the orientation of the lens trajectory with respect to the axis of rotation.

[2] Note that for rotation, v_0 is limited by the rotational speed of breakup, whereas expanding winds typically have terminal speeds significantly in excess of the stellar escape speed. Hence the line width can provide a distinction between the two cases, unless the expansion speed happens to be somewhat small.

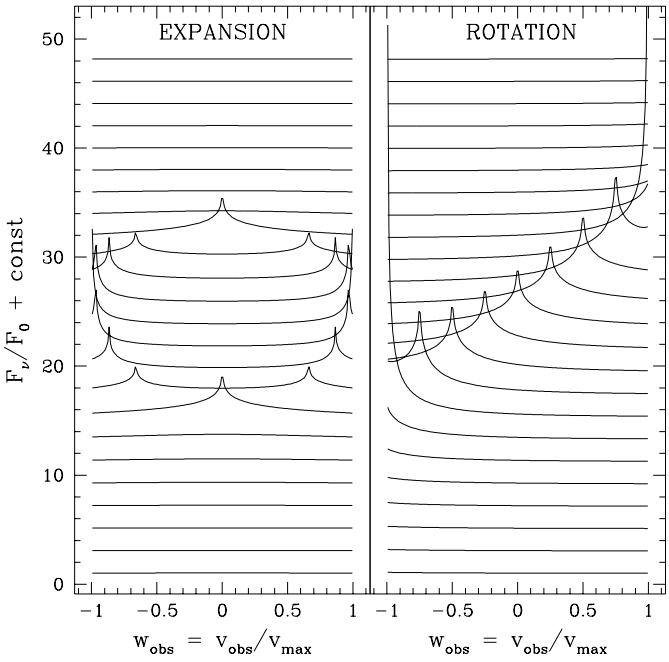

Fig. 3. Shown are simulations of the microlensing of a uniformly expanding shell (*left*) and a uniformly rotating shell (*right*). In this calculation the shell radius is equal to the Einstein radius and the lens is taken to transit the center of the shell. Additionally, the lens trajectory is orthogonal to the projected axis of rotation. A constant offset has been applied between the profiles to better show the time evolution of the line shape (time increasing upwards). Note that in the expansion case, the line emission is symmetric about line center at all times; for rotation the profile is distinctly asymmetric.

Table 1. Lens parameters for the model line profiles

$d_{\rm sh}$	d_0	γ	$A_{\rm max}$		$f_{\rm line}$		Figure
			Exp	Rot	Exp	Rot	
0.3	0.0	270°	33.4	83.1	5.3	3.2	4
	0.3	270°	13.6	9.2	5.3	2.4	4
	1.0	270°	1.4	1.4	1.4	1.3	4
1.0	0.0	270°	10.0	36.9	1.9	2.1	3,5
	0.3	0°	7.1	6.4	1.9	2.1	7
	0.3	45°	7.1	9.6	1.9	2.1	7
	0.3	270°	7.1	8.5	1.9	2.1	5
	0.3	315°	7.1	9.6	1.9	2.1	7
	1.0	270°	4.6	3.7	1.9	1.6	5,7
3.0	0.0	270°	4.5	16.0	1.2	1.5	6
	0.3	270°	9.4	9.1	1.2	1.5	6
	1.0	270°	2.3	3.7	1.2	1.4	6

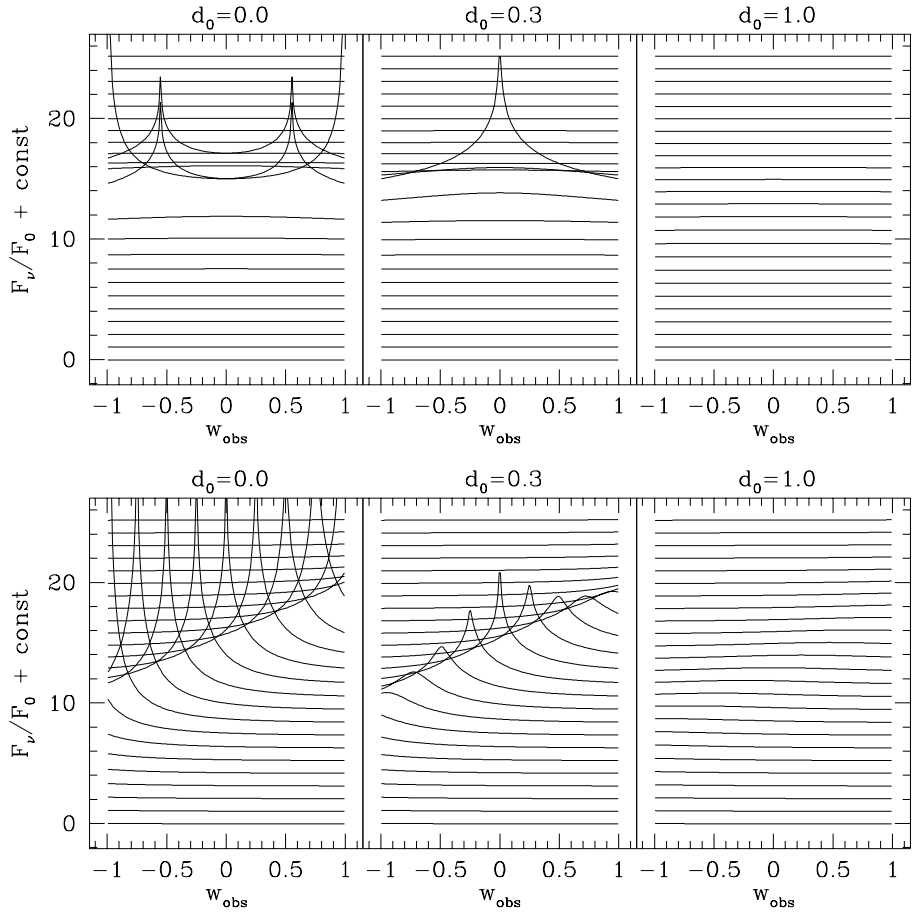

Fig. 4. With expansion for the upper panels and rotation for the lower panels, this figure shows the time evolution of the line shape for $d_{\rm sh} = 0.3$. From left to right, the different cases are for impact parameters d_0 as indicated. Note that for this relatively small value of $d_{\rm sh}$ strong microlensing effects occur, but only for timesteps corresponding to small impact parameters.

2.2.1. Expansion versus rotation

Fig. 3 contrasts the microlensed line profiles from an expanding shell (left) to one that is rotating (right), where the observed velocity shift is $v_{\rm obs} = v_{\rm Z}$ and the maximum velocity shift $v_{\rm max}$ is equal either to v_0 for expansion or $v_0 \sin i$ for rotation. In this simulation we have chosen $d_{\rm sh} = r_{\rm sh}/r_{\rm E} = 1.0$, where $r_{\rm sh}$ is the angular stellar radius. The lens is taken to transit the shell across the line-of-sight to the shell center with minimum impact parameter $d_0 = 0$. In the case of rotation, we have further assumed that the lens trajectory is orthogonal to the projection of the rotation axis in the plane of the sky. The two panels show a sequence of line profiles, beginning with the lens at a projected distance of $3r_{\rm E}$ from the centre of the shell, which then decreases to zero and increases back to $3r_{\rm E}$ on the opposite side of the shell. Results are plotted as the ratio of the lensed flux, F_ν, to the unlensed flux, F_0 (the latter being just the flat-top profile), plus a constant offset introduced between each timestep to better display the time evolution of the profile shape.

From Fig. 3, it is evident that the microlensed profiles for an expanding shell are distinctly different from those of a rotating shell. For expansion the profile shape is symmetric both in velocity about line center and in time with respect to the lens position at impact parameter d_0. In contrast, the profile shape in the rotating case is not symmetric in velocity, and although it is symmetric in time for the lens trajectory assumed in Fig. 3, the profile evolution is not time symmetric in general, as will be shown in Sect. 2.2.3.

The difference between the expansion and rotation cases for the microlensed line profile evolution can be understood from considerations of the bulk flow properties of the two cases. A sightline from the observer to the lens will intersect the shell at two points: one in the front hemisphere and one in the back. As note previously, the observed Doppler shift at these two points is equal in magnitude but opposite in sign for expanding shells, thereby resulting in an amplification at predominantly two points in the profile, with the two points being equidistantly located from line center. However, for a rotating shell, the Doppler shifts at the two intersection points are equal both in magnitude and direction, hence the amplification of line emission occurs predominantly at only one point in the line – resulting in the asymmetric profile shapes.

2.2.2. Variation of $d_{\rm sh}$

Figs. 4–6 demonstrate how the variation of $d_{\rm sh}$ affects the response of the line profile to microlensing. The three figures are respectively for $d_{\rm sh} = 0.3$, 1.0, and 3.0. Each plot shows six panels, with the upper set for an expanding shell and the lower one for a rotating shell. As labelled, the different panels correspond to different impact parameters of the lens, with values of $d_0 = 0.0$, 0.3, and 1.0. Note that as in the previous section, we

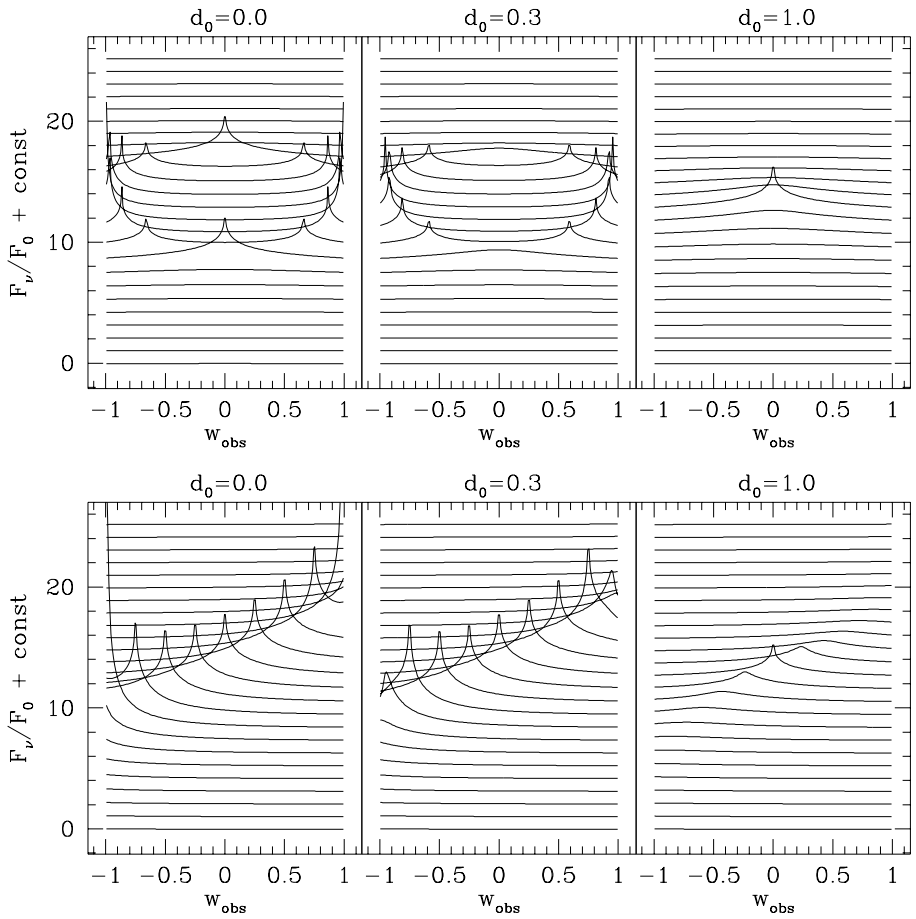

Fig. 5. As Fig. 4 but with $d_{\rm sh} = 1.0$. As compared to the case of $d_{\rm sh} = 0.3$, interesting microlensing effects now persist for a broader range of d_0; however, the greatest amplifications no longer achieve the highest values obtained with smaller $d_{\rm sh}$.

assume that the lens trajectory intercepts the projected axis of rotation at a right angle.

Increasing $d_{\rm sh}$ leads to three primary effects for the lensed line profiles:

- The maximum amplification of the emission line becomes smaller with increasing values of $d_{\rm sh}$. For more "compact" shells, as characterised by smaller $d_{\rm sh}$, the amplification is strongly concentrated to the regions of the shell lying most nearly behind the lens, which leads to the rather "spikey" profiles seen in Fig. 4. For sources which are less compact, as in Figs. 5 and 6, the peak amplification is significantly reduced (refer to $A_{\rm max}$ in Table 1).
- Another interesting effect apparent from Figs. 4 – 6 is that for small $d_{\rm sh}$, significant microlensing results only for lens trajectories with small d_0, whereas larger $d_{\rm sh}$ show interesting profile effects even for values of $d_0 \gtrsim 1.0$. This result is more easily understood if we consider d_0 relative to $d_{\rm sh}$. Consider the rightmost panels of Fig. 4. Although the minimum impact parameter equals the Einstein radius, d_0 is more than three times greater than $d_{\rm sh}$, hence the lens does not actually transit the shell, explaining why an essentially flat-top profile persists for both expanding and rotating shells. Conversely, we see from Fig. 6 that significant lensing is apparent for $d_0 = 1.0 = d_{\rm sh}/3$; this is not surprising since in this case the lens actually transits the shell. The important conclusion is that significant microlensing is expected in the line profiles whenever the trajectory of the lens intersects the extended shell.
- Fig. 6 indicates that for $d_{\rm sh} = 3$, there is little to distinguish between the line profile evolution for the chosen minimum impact parameters. There are certainly some detailed differences between the simulations, such as the maximum amplification, yet the overall time response and average amplification appear quite similar between the different runs. This similarity reflects the fact that $d_{\rm sh}$ is relatively large compared to d_0 for these three cases. The line profile shape is more sensitive to the value of d_0 for smaller values of $d_{\rm sh}$, as is clear from Figs. 4 and 5.

2.2.3. Variation of the lens position angle

In discussing the position angle, γ, of the lens trajectory, we are not concerned with the case of spherically symmetric expanding shells, for which the microlensing effects are independent of γ at fixed d_0. However, this is not the case for a rotating shell, because even if the shell density is spherical, the isovelocity zones in the rotating case are not axially symmetric about the line-of-sight (except for a pole-on viewing perspective).

Fig. 7 shows microlensed line profiles for four values of $\gamma = 0°$, $45°$, $270°$, and $315°$. The position angle is measured counterclockwise from the Y–axis which is assumed coincident

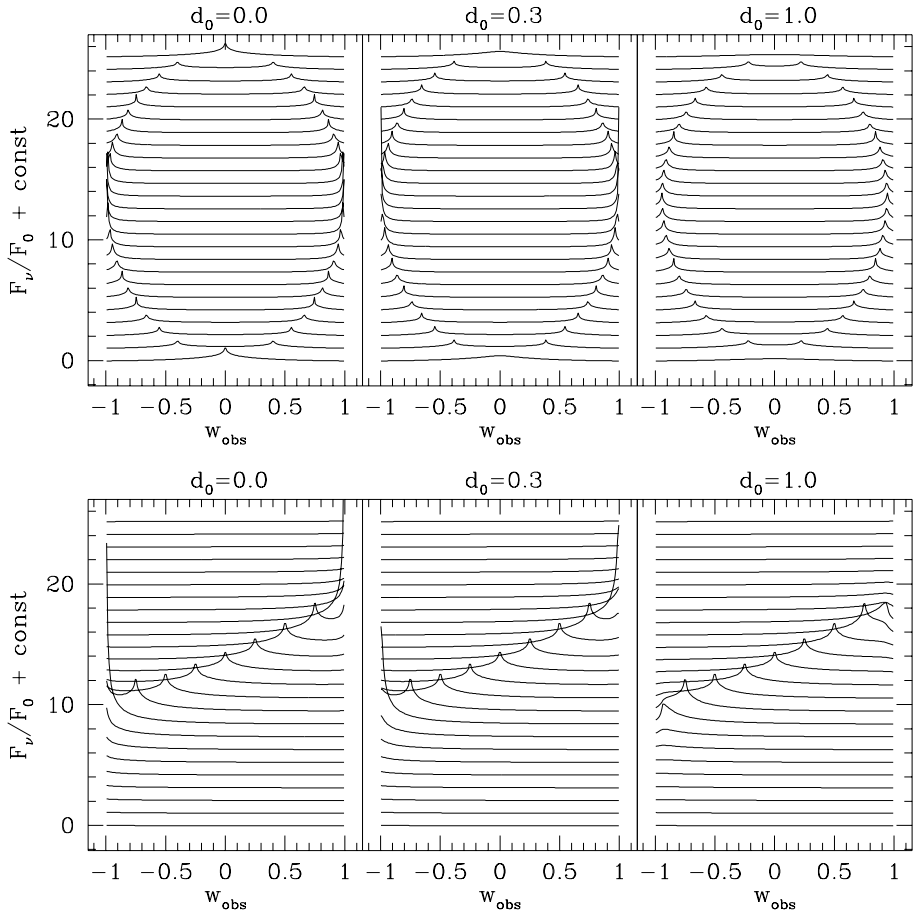

Fig. 6. As in Figs. 4 and 5, but for $d_{\rm sh} = 3.0$. Now the effects of microlensing can be seen for quite a large range of d_0 but the amplifications are further reduced compared to those for the smaller values of $d_{\rm sh}$. Note also that, since $d_{\rm sh}$ is large compared with d_0, there is little to distinguish between results for the three different values of d_0.

with the projected axis of rotation. Hence, $\gamma = 0^\circ$ runs parallel to the projected rotation axis in the direction bottom to top, and $\gamma = 270^\circ$ runs orthogonal to that axis from left to right. The simulations are for fixed values of $d_{\rm sh} = 1.0$ and $d_0 = 0.3$.

Let us first compare the two cases of $\gamma = 0^\circ$ and 270°. Recall that the isovelocity zones are circular rings that are seen as linear strips in projection, thus for $\gamma = 0^\circ$, the lens trajectory runs along the strip with $d_0/d_{\rm sh} = 0.3$, corresponding to $w_{\rm obs} = 0.3$. Consequently, the peak amplification always appears at this velocity shift in the profile. For $\gamma = 270^\circ$, the lens transits each isovelocity strip, and the result, as in the previous figures, is that the peak amplification smoothly migrates across the line profile with time.

Now for lens trajectories that are oblique relative to the rotation axis (as is the case for $\gamma = 45^\circ$ and 315°), the lens does not transit all of the isovelocity strips. Neither does the lens position at minimum impact parameter lie along the isovelocity strip of zero velocity shift. The consequence as seen in Fig. 7 is that the peak amplification moves smoothly across the profile but is significantly greater than unity only for those velocity shifts where the corresponding isovelocity zones are transitted by the lens. Further, we have plotted as dashed the line profile corresponding to when the location of the lens is at d_0. The peak amplification at this time is not at line center, because the lens position does not lie on the isovelocity strip of zero Doppler shift. The evolution of the peak amplification relative to this time is different for $\gamma = 45^\circ$ than for 315°. We conclude that the value of γ may be recovered from the profile evolution by virtue of where the peak amplification occurs in the line profile when the lens is at the position of minimum impact parameter combined with how the peak amplification evolves across the line relative to that time.

3. Discussion

This paper has focussed on the effects of microlensing for the shapes of emission line profiles from expanding or rotating extended spherical shells. From the line profile simulations, it appears that microlensing, which is normally used as a means of constraining the properties of the lens, provides a unique and powerful probe of the stellar source environment. We find that microlensing can be used to infer the velocity field of the flow, the values of $d_{\rm sh}$ and d_0, and the orientation of the lens trajectory γ in the case of rotation.

3.1. Observational prospects

The introduction of event alert programs in many of the microlensing surveys allows to acquire spectroscopic observations at visible wavelengths of the source star *during* the microlensing event. Benetti et al. (1995) were the first to obtain such spectra; however, the source in this case was relatively faint, with

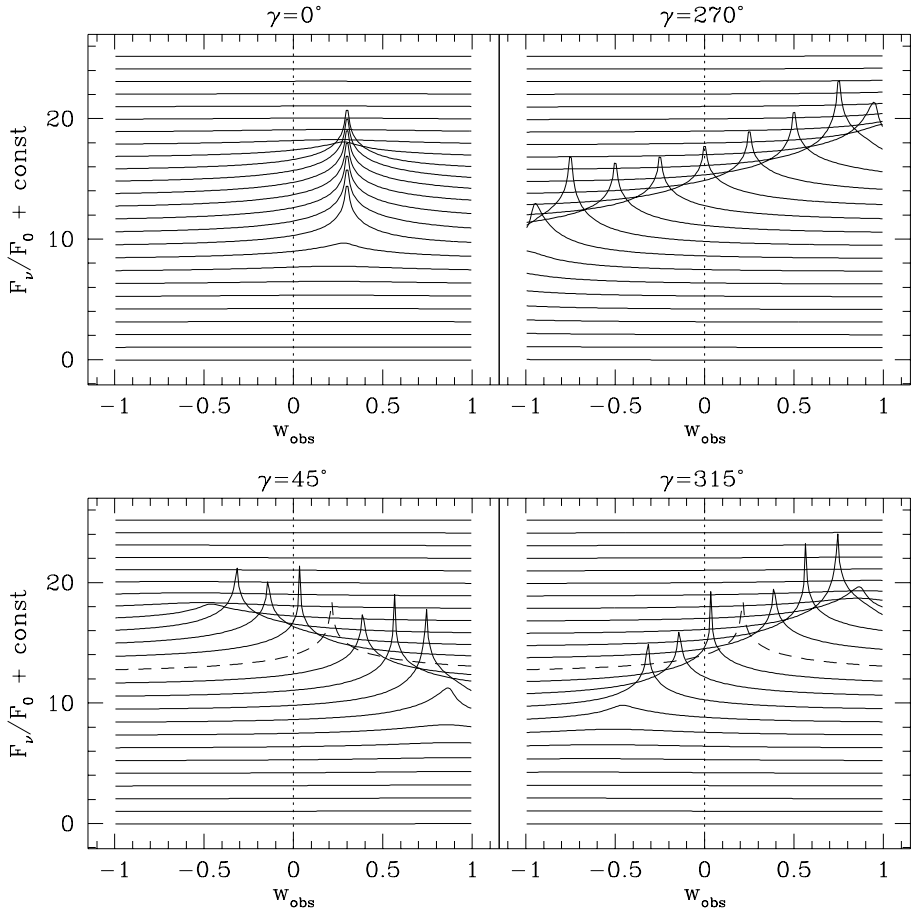

Fig. 7. Shown are microlensing simulations for a rotating shell with $d_{\rm sh} = 1.0$ and $d_0 = 0.3$ but allowing the position angle γ of the lens trajectory to vary. The angle γ is measured counterclockwise from the rotation axis, hence $\gamma = 0^\circ$ is a trajectory parallel to the rotation axis and $\gamma = 270^\circ$ is one that is orthogonal to the rotation axis with the lens moving left to right. These simulations indicate that the relative trajectory of the lens can be recovered from the evolution of the profile shape. Note especially that for $\gamma = 45^\circ$ and 315°, the profile corresponding to the lens' closest approach is plotted as dashed. It is evident that evolution of the line profile is not symmetric in time, a result that is explained more fully in text.

an unlensed magnitude of $V = 20$, and their data were of low resolution ($\sim$ 13 Å). Higher resolution ($\sim$ 5 Å) spectra were obtained with 2 and 4 meter telescopes of the one definitive detection of extended source effects reported by Alcock et al. (1997; MACHO 95–30). These two cases were for microlensing candidates in the bulge. Spectroscopy has also been acquired by Beaulieu et al. (1995) for 19^{th} magnitude candidates in the LMC, although these observations were not made during the event but as a follow-up.

It is clear that spectroscopy of the source star during a microlensing event is already feasible with current observational limits and can provide crucial additional information about both the lens and the source. It remains to consider, however, the frequency with which observations of extended effects can be expected. One can estimate this frequency by considering the fraction of candidate events which are transits (i.e., with angular impact parameter less than the angular source radius) given that their peak amplification exceeds the detection threshold (i.e., $d_0 \leq 1$) currently adopted by the microlensing surveys. As noted by Valls-Gabaud (1998), a crude estimate of this fraction, f, is given by

$$f \quad = \quad \langle r \rangle \, \langle 1/r_{\rm E} \rangle \tag{10}$$

where $\langle r \rangle$ is the typical angular size of the source. Assuming that giant stars account for a third of lensing sources and have radii of $10R_\odot$ and further that lenses have masses of $0.1M_\odot$, Valls-Gabaud estimated $f \approx 10\%$ for sources in the bulge. This fraction is halved if one adopts a lens mass of $0.5M_\odot$, which is more typical of the present survey results. Note, however, that the estimate of f is proportional to $\langle r \rangle$, and adopting $\langle r \rangle = 10R_\odot$ is the appropriate number only for the *photospheric* sizes of the source stars. Hence the estimated fraction could be substantially increased when the larger radius of the circumstellar envelope taken into account.

With regard to the observed event rate, reference has already been made to the observation of finite source effects in MACHO 95–30 (Alcock et al. 1997), but this star does not stand alone, as other examples of high amplification (i.e., small d_0) or short duration (i.e., low lens mass) events exist that are also suggestive of finite source effects (Mao et al. 1994; Lennon et al. 1996; Bennett et al. 1997; Pratt 1997). More recently, MACHO alert 98-BLG-35 (c.f., http://wwwmacho.anu.edu.au/) has been observed to have a peak amplification of 70.6; with such a large value, it is a prime candidate to look for finite star effects. Thus, out of over a hundred microlensing candidates, there exist about a handful of events with confirmed or suspected extended source effects, which is consistent with the above estimation.

3.2. Beyond simple shells

Although our treatment here has been highly simplified, this work represents an initial investigation into a broad range of di-

agnostics for circumstellar envelope structure from microlensing events. Here we summarize avenues of future research on this topic:

– Previous work on stellar photospheres (c.f., Gould & Welch 1996; Valls-Gabaud 1998; Coleman 1998; Hendry et al. 1998) has shown that microlensing is a unique probe of atmospheric limb darkening, because the effective stellar radius is a function of wavelength. In the same way, the effective radius of circumstellar envelopes is also a function of wavelength. The line formation region of some ions is considerably more extended than for others (see below), and different continuum emission processes vary in their dependence on parameters such as density and temperature (also see below). If observed in the appropriate wavebands, a circumstellar envelope can present a much larger geometric cross-section than does the stellar photosphere alone. This is advantageous for the detection of microlensing events, given that significant amplification will be observed only if the emitting region lies within $r_{\rm E}$ of the lens. Consider in particular red giant stars, which compose around 20% of the stars observed by OGLE in the direction of the Galactic bulge (Loeb & Sasselov 1995), thus comprising a major fraction of their candidate microlensing events. Some of these objects have dust driven outflows, and the dust envelopes produce significant emission at infrared wavelengths corresponding to geometric sizes of several stellar radii. Consequently, microlensing monitoring programs that target the infrared wavebands should expect a higher incidence of lensing events as compared to just B,V or R bands.
– We have explored the effects of microlensing only for uniformly expanding or rotating shells and found that microlensing can provide valuable information about the velocity field. For more realistic extended envelopes (e.g., accelerating winds or Keplerian disks), we anticipate that microlensing will not only yield the direction of the flow but also information on the radial derivative. For example, a Keplerian disk has slow rotational speeds at large radii and rapid rotational speeds at small radii. During a microlensing event, we would therefore expect the peak amplification to appear first near line center, migrate toward one extreme wing, then rapidly migrate to the other wing as the lens moves to the opposite side of the disk, and finally return to line center as the event concludes. In contrast, a very different behavior is anticipated if the rotation were to increase with radius (e.g., solid body rotation), for which the speed of rotation is largest at the radius of greatest extent than at the inner regions. The line profile would evolve in a manner similar to our results for uniformly rotating shells, with the peak amplification appearing first at one extreme wing and migrating across the profile to the opposite wing. These two examples assume $\gamma = 270^\circ$, but similar arguments can be made for other lens trajectories. The essential idea is to consider how the lens overlaps different isovelocity zones as it tracks across the sky. Microlensing presents a tremendous opportunity to distinguish between expansion and accretion and to infer the angular momentum distribution of lensed envelopes.
– With spectral monitoring during a microlensing event, one could make relative comparisons of the time evolution in lines of different ions. Such measurements allow to determine the ionization distribution throughout the wind by virtue of the relative time intervals in the amplifications of different lines. A natural expectation is that higher ionization species will exist at smaller radii, closer to the star, than will lower ionization species. The lines should have emission line equivalent widths that are increased by the microlensing such that the light curves for lines formed at small radii have smaller FWHM than those formed over a greater radial extent. A multiline approach provides a tool of measuring just how stratified the ionization distribution is.
– A similar issue is how the continuum emission evolves during a microlensing event. There are a variety of continuum emission processes that may operate in an extended envelope, but at different spatial locations. For example, some carbon rich Wolf-Rayet stars show (a) dust formation that is occuring at large radius (Williams et al. 1987), (b) free-free dominated radio and infrared excesses over an extended region, and (c) a pseudo-photosphere dominated by electron scattering at shorter wavelengths. For such a star, one expects that during a microlensing event the dust shell is amplified at far-infrared wavelengths, then amplification of the continuum emission appears at progressively shorter wavelengths up until the lens reaches its minimum impact parameter, after which the amplification subsides in the reverse order. An especially interesting aspect of this case is that the amplification at the shortest wavelengths yields information on the effective stellar radius. This radius can in turn be used to measure the relative extent of the continuum emission throughout the envelope. The continuum formation will have some dependence on density (e.g., free-free emission depends on the square of the density), so that the microlensed data can be used to infer the radial velocity in the flow. These kinds of considerations can also be applied to other types of hot star winds and to the outflows of evolved late type stars.
– The previous discussion has implicitly assumed rather smoothly flowing envelopes, but it is well-known that at least hot star winds have a considerable level of structure, or "clumpiness" (Conti 1988; Henrichs 1988). A detailed analysis of the broad band photometric light curve during a microlensing event may provide information about the scale and frequency of such clumpy structures, particularly if $r_{\rm E}$ is of order the angular scale of the clumps. Theoretically, the development of a diagnostic to probe the clumpiness of circumstellar envelopes bears some similarity to problems involving the microlensing of photospheres with spots that have been investigated by Hendry & Valls-Gabaud (in prep).
– Lastly, (spectro-) polarimetric observations during a microlensing event would provide especially detailed information about the circumstellar envelope structure. For the pur-

pose of discussion, consider only polarisation arising from Thomson scattering. The degree of polarisation for any single scattering depends on the scattering angle and is largest for right angle scattering. The convolution of the emergent polarised light with the lens amplification factor is therefore localized to spatial regions in the vicinity of the plane of the sky (i.e., where the scattering angle is nearly $90°$) and insensitive to regions where the scattering is nearly forward ($0°$) or backward ($180°$) scattering. As a result, the polarimetric light curve of a microlensing event is a more sensitive tracer of the radial structure of the envelope. Such data may provide an even better diagnostic of clumpiness than the intensity light curve approach discussed previously. Moreover, since the number of scatterers depends on the density (with a linear dependence), the light curve will also provide information about the radial velocity distribution.

There are clearly several tacts for future diagnostic development in this highly interesting field. Of particular note is the potential extension of the methods discussed in this paper to the microlensing of quasars and AGN environments. Observational evidence for quasar microlensing, based on monitoring the long term variability of broad band quasar light curves, has been reported by Hawkins (1993, 1996), although the microlensing interpretation remains somewhat controversial and several authors have favoured intrinsic quasar variability as the more likely paradigm (c.f., Wallinder et al. 1992; Baganoff & Malkan 1995). Spectroscopic diagnostics based on modification of both emission and absorption lines of quasars and AGN during a microlensing event have been investigated in numerous studies (c.f., Nemiroff 1988; Schneider & Wambsganss 1990; Gould & Miralda-Escude 1997; Lewis & Belle 1998), which conclude that microlensing can provide an important probe of density and velocity structure in AGN environments. In relation to the results of this paper, Arav et al. (1995) has applied the line-driven wind theory of hot stars to interpret the broad absorption lines of quasars, which indicates that the diagnostic techniques presented here for probing stellar envelopes may also have relevance to AGN. In particular, spectral diagnostics may provide an unambiguous signature of quasar microlensing over a range of lens masses, in which case microlensing observations may be used to study different components of AGN in considerable detail.

In conclusion, the techniques, results and discussion presented here clearly suggest that microlensing provides a powerful new tool for diagnosing the density and velocity structure of extended circumstellar envelopes. We will describe the application of these techniques to more realistic stellar models, and to quasars and AGN, in subsequent papers.

Acknowledgements. The authors wish to express their appreciation to Drs. J.E. Bjorkman, N. Gray, and D. Valls-Gabaud for valuable discussions on the microlensing of circumstellar envelopes. Thanks also to an anonymous referee for suggestions that have improved this paper. This research was funded by a PPARC rolling grant.

References

Alcock C., Axerloff C.W., Allsman R.A., et al., 1993, Nat 365, 621
Alcock C., Allsman R.A., Axelrod T.S., et al., 1995, AJ 109, 1653
Alcock C., Allsman R.A., Axelrod T.S., et al., 1996, ApJ 461, 84
Alcock C., Allen W.H., Allsman R.A., et al., 1997, ApJ 491, 436
Alcock C., Allsman R.A., Alves D.R., et al., 1998, ApJ 492, 190
Arav N., Korista K.T., Barlow T.A., Begelman M.C., 1995, Nat 376, 576
Aubourg E., Bareyre P., Brehin S., et al., 1993, Nat 365, 623
Baganoff F.K., Malkan M.A., 1995, ApJ 444, L13
Beaulieu J.P., Ferlet R., Grison P., et al., 1995, A&A 299, 168
Benetti S., Pasquini L., West R.M., 1995, A&A 294, L37
Bennett D.P., Alcock C., Allsman R.A., et al., 1997. In: Soderblom D.R. (ed.) Planets Beyond the Solar System and the Next Generation of Space Missions, San Francisco: ASP, p. 95
Coleman I.J., 1998, Ph.D. Thesis, University of Glasgow
Conti P.S., 1988, In: Conti P.S., Underhill A.B. (eds.) NASA SP-497, O Stars and Wolf-Rayet Stars, p. 137
Gould A., 1994, ApJ 421, L71
Gould A., Miralda-Escude, J., 1997, ApJ 483, L13
Gould A., Welch D., 1996, ApJ 464, 212
Grison P., Bealieu J.-P., Pritchard J.D., et al., 1995, A&AS 109, 447
Hawkins M.R.S., 1993, Nat 366, 242
Hawkins M.R.S., 1996, MNRAS 278, 787
Hendry M.A., Coleman I.J., Gray N., Newsam A.M., Simmons J.F.L., 1998, New Astronomy Reviews, in press
Henrichs H., 1988, In: Conti P.S., Underhill A.B. (eds.) NASA SP-497, O Stars and Wolf-Rayet Stars, p. 199
Heyrovský D., Loeb A., 1997, ApJ 490, 38
Lennon D.J., Mao S., Fuhrmann K., Gehren T., 1996, ApJ 424, L21
Lewis G.F., Belle K.E., 1998, MNRAS 297, 69
Loeb A., Sasselov D.D., 1995, ApJ 449, L33
Mao S., di Stefano R., Alcock C., et.al, 1994, BAAS 185, 1705
Menzel D.H., 1929, PASP, 41 344
Mihalas D., 1978, Stellar Atmospheres, (Freeman: New York)
Nemiroff R., 1988, ApJ 335, 593
Newsam A.M., Simmons J.F.L., Hendry M.A., Coleman I.J., 1998, New Astronomy Reviews, in press
Paczyński B., 1986, ApJ 304, 1
Paczyński B., 1996, ARA&A 34, 419
Peng E.W., 1997, ApJ 475, 43
Pratt M.R., 1997, In: Proc. 2nd. Internat. Workshop on Gravitational Microlensing Surveys (Orsay: LAL-Orsay), 243
Sasselov D., 1997, In: R. Ferlet (ed.) IAP Colloq. Variable Stars and the Astrophysical Returns of Microlensing Surveys, in press
Schneider P., Wambsganss J., 1990, A&A 237, 42
Simmons J.F.L., Newsam A.M., Willis J.P., 1995a, MNRAS 276, 182
Simmons J.F.L., Willis J.P., Newsam A.M., 1995b, A&A 293, L46
Udalski A., Szymanski M., Kaluzny J., et al., 1993, Acta Astron. 43, 289
Udalski A., Szymanski M., Kaluzny J., Kubiak M., 1994, Acta Astron. 44, 1
Valls-Gabaud D., 1994, In: Mücket J. et al. (eds.) Large Scale Structures in the Universe, (World Scientific) p. 326
Valls-Gabaud D., 1998, MNRAS, 294 747
Wallinder F.H., Kato S., Abramowicz M.A., 1992, A&AR 4, 79
Williams P.M., van der Hucht K.A., The P.S., 1987, A&A 182, 91